2011-09

Development of the 'MN''SI IND. 1.7' phase in 'MN'-containing 'SI' films

Materials Chemistry and Physics,Lausanne : Elsevier, v. 129, n. 1/2, p. 148-153, Sept. 2011
http://www.producao.usp.br/handle/BDPI/49511

Materials Chemistry and Physics 129 (2011) 148–153

Contents lists available at ScienceDirect

Materials Chemistry and Physics

journal homepage: www.elsevier.com/locate/matchemphys

Development of the $MnSi_{1.7}$ phase in Mn-containing Si films

F.A. Ferri [a,*], M.A. Pereira-da-Silva [a,b], A.R. Zanatta [a]

[a] Instituto de Física de São Carlos – USP, São Carlos 13560-250, SP, Brazil
[b] Centro Universitário Central Paulista – UNICEP, São Carlos 13563-470, SP, Brazil

ARTICLE INFO

Article history:
Received 19 August 2010
Received in revised form
13 December 2010
Accepted 27 March 2011

Keywords:
A. Thin films
B. Sputtering
C. Raman spectroscopy and scattering
D. Microstructure

ABSTRACT

Thin films of Si with Mn concentrations up to 20 at.% were prepared by conventional radio frequency sputtering. After deposition, the films were submitted to thermal annealing treatments and their properties were investigated by composition analysis, Raman scattering, microscopic techniques, optical transmission, and electrical transport. The experimental results show that all as-deposited films are amorphous, with the Mn atoms being effective and controllably incorporated into the Si matrix. Moreover, thermal annealing at increasing temperatures induces the crystallization of the films as well as the growth of the $MnSi_{1.7}$ silicide phase in the Mn-containing samples. Along with sample crystallization, some films become covered by small structures that are randomly distributed all over their surfaces. These structures are essentially Mn-containing Si crystals with typical sizes in the (sub-) micrometer range and, as the thermal annealing advances, the density of structures increases at the expense of their individual average dimension. The development and characteristics of the observed superficial structures are discussed in view of the main structural and morphological properties of the samples.

1. Introduction

Basic and applied research involving ferromagnetic semiconductors (FMS's) have gained renewed attention along the last few years mainly because of their prospects in spin-based electronics or, simply, *spintronics*. Practical applications in this field require the manipulation of both the charge and spin of electrons, which are expected to produce devices such as nonvolatile high density memories, sensitive sensors, and spin field-effect transistors – just to mention a few of them [1]. Indeed, the achievement of *spintronic* devices is frequently considered in the studies of II–VI or III–V compounds doped with transition metal elements [2].

More recently, and aiming at the development of FMS materials, compatible with the existing (micro-) electronics industry, group-IV semiconductors doped with manganese have also been considered in detail [3–5]. However, the insertion of manganese into crystalline group-IV semiconductors was found to be very much limited [6,7]. Usually, the manganese concentration is low, its distribution is not homogeneous and, consequently, the origin (or absence) of magnetic activity in these materials is not always straightforward. Part of these problems can be avoided by using amorphous (*a*-)Si or *a*-Ge matrices in which the inherent structural metastability increases the solid solubility of foreign species [8–10]. In fact, it is well-established that a large amount of manganese can be incorporated into *a*-Si and *a*-Ge compounds which can exhibit a more homogenous distribution and, eventually, magnetic activity [11–14].

The technological potential of the SiMn or GeMn systems, however, is not restricted to the field of *spintronics*. The association of many desirable characteristics (resistance to corrosion, superior thermal stability and electrical properties) exhibited by certain transition-metal silicides, for example, make them well-suited for applications in very-large-scale-integration circuits: acting either as ohmic contacts or Schottky barriers [15,16].

Motivated by the above aspects, this work reports on the synthesis and spectroscopic–microscopic investigation of SiMn thin films prepared by sputtering. In fact, this work adds-up valuable information to a previous communication in which only the magnetic properties of the SiMn (with [Mn] ~ 20 at.%) film were investigated in detail [14]. In this respect, the present contribution discusses the development of (sub-)micrometer structures on the surface of the thermally annealed SiMn films as well as their main structural–morphological characteristics.

2. Experimental details

All SiMn films considered in this study were deposited by radio frequency (13.56 MHz) sputtering a poly-crystalline Si target (99.999% pure) in an atmosphere of argon (99.999% pure). Taking advantage of the sputtering method, the insertion of Mn was achieved by partially covering the Si target with suitable pieces of metallic Mn (99.999% pure). In such a case, the variation of the relative Mn-to-Si target area allows the control of the metal concentration into the samples. Films with [Mn] up to 20 at.% were prepared. For comparison purposes, one Mn-free Si film was also deposited following the same experimental conditions. The films, typically

* Corresponding author.
E-mail address: ferri@ursa.ifsc.usp.br (F.A. Ferri).

0254-0584/$ – see front matter © 2011 Elsevier B.V. All rights reserved.
doi:10.1016/j.matchemphys.2011.03.064

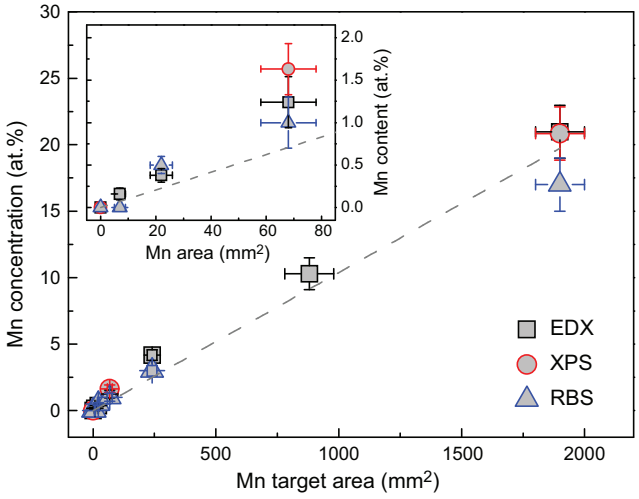

Fig. 1. Manganese concentration of SiMn films, as-deposited, as a function of the target area covered with Mn during deposition. As indicated in the figure, the [Mn] was achieved by energy dispersive X-ray spectrometry (EDX), X-ray photoelectron spectroscopy (XPS), and Rutherford backscattering (RBS) measurements. The inset shows details of the Mn concentration for Mn target areas in the 0–80 mm² range. The dashed straight lines are just guides to the eye.

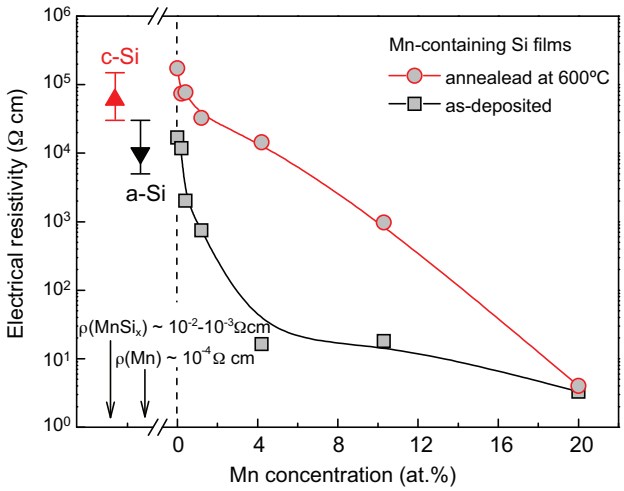

Fig. 2. Electrical resistivity of SiMn films ([Mn] ~ 0–20 at.%) as determined from the van der Pauw method (at room temperature and dark conditions). The data refer to films as-deposited and after thermal annealing at 600 °C. The electrical resistivity values corresponding to undoped silicon (both *c*-Si and *a*-Si), silicon-manganese alloys ($MnSi_x$), and metallic manganese (Mn) are also indicated for comparison purposes. The lines joining the experimental data points are just guides to the eye.

1700 nm thick as indicated by profilometry measurements, were deposited onto different substrates (*c*-Si, *c*-Ge, *c*-quartz, and glass) kept at 150 °C. After deposition the films were thermally annealed in the 300–900 °C temperature range under a continuous flow of argon. The thermal treatments were isochronal (15 min each) in steps of 150 °C.

The manganese concentration in the films was determined independently by means of: (1) energy dispersive X-ray spectrometry EDX (from a 20 keV electron beam), (2) Rutherford backscattering RBS (by means of a 3 MeV He^+ beam impinging normal to the sample surface), and (3) *ex-situ* X-ray photoelectron spectroscopy XPS (under ultrahigh-vacuum conditions and 1486.6 eV photons provided by an Al Kα X-ray source). Typically, the sample analyzed areas by each of these techniques were: ~100 μm × 100 μm (EDX), 1 mm × 1 mm (RBS), and 3 mm × 3 mm (XPS). In order to remove unintentional contaminants (mainly oxygen) from the surface of the samples, all XPS measurements were preceded by 3 min sputtering with Ar^+ ions (500 eV).

The atomic structure of the films was investigated through Raman spectroscopy under the backscattering geometry. The measurements were carried out at room temperature with 632.8 nm photons (HeNe laser). Sample areas around 1 μm² were analyzed using an average power density of ~200 μW μm^{-2}.

The surface morphology of the SiMn films was investigated with the help of scanning electron (SEM) and atomic force (AFM) microscopy techniques.

3. Results and discussion

The manganese concentration of the samples (as-deposited) considered in the present study is shown in Fig. 1. The figure displays the results obtained from EDX, RBS and XPS measurements as a function of the Mn target area employed during deposition. As can be seen, the results obtained by the different techniques are in good agreement. It is also evident from Fig. 1 that the manganese atoms were effective and controllably incorporated into the Si matrix and that the Mn content scales with the target area covered with Mn. Moreover, EDX measurements taken at different regions indicate that the manganese atoms are homogeneously distributed in the as-deposited films.

Just like any other Si-based compound, the optical–electronic properties of the SiMn films are influenced by the presence (and quantity) of impurities as well as by post-deposition treatments. Part of these effects can be noticed through the electrical resistivity values (Fig. 2) and optical transmission data (Fig. 3) obtained from Si films containing different Mn concentrations: as-deposited and after thermal annealing at 600 °C.

The electrical resistivity (ρ) of the SiMn films was obtained from the van der Pauw method (at room temperature and dark conditions) [17] and is presented in Fig. 2. The ρ values of undoped crystalline [18] and amorphous Si [8], $MnSi_x$ compounds [16], and metallic Mn [19] are also shown for comparison. In the amorphous form (as-deposited films in Fig. 2) the electrical processes taking place in the films are dominated by a large amount of defects [20]. The presence of manganese into the *a*-Si matrix increases the density of defects and, consistently, ρ experiences a variation of almost three orders of magnitude with the insertion of approx. 4 at.% of Mn. A similar reasoning applies to the films after annealing at 600 °C. In such a case, however, the variation of the ρ values is less abrupt and the electrical processes are determined by the presence of defects and by the appearance of a Mn-related deep level in the Si matrix [18,21]. Also, and as will be discussed in the following, annealing the films at 600 °C induces the development of the $MnSi_{1.7}$ silicide phase which, certainly, affect the overall electrical behavior of

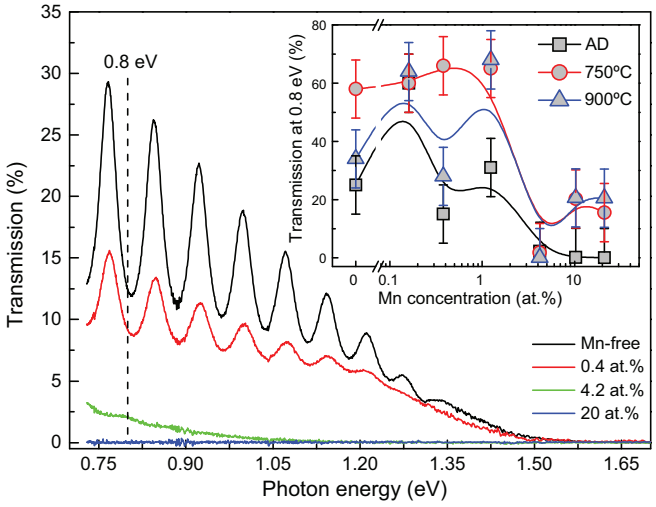

Fig. 3. Optical transmission spectra of some SiMn films ([Mn] = 0, 0.4, 4.2, and 20.0 at.%) deposited on crystalline quartz substrates. The spectra refer to samples as-deposited (AD) and the fringes apparent in the spectra of the Mn-free and with [Mn] = 0.4 at.% films are due to interference effects. The inset shows the average optical transmission (at the arbitrarily chosen energy of 0.8 eV) as a function of the Mn concentration of the films: as-deposited and after thermal annealing at 750 and 900 °C.

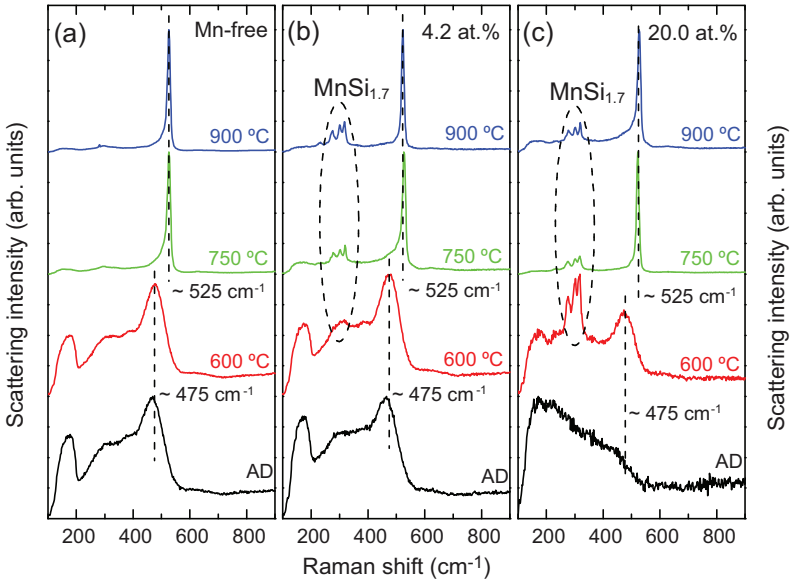

Fig. 4. Raman spectra of SiMn films: as-deposited (AD) and after thermal annealing at 600, 750, and 900 °C. The spectra correspond to the following samples: (a) Mn-free, (b) containing 4.2 at.% of Mn, and (c) containing 20.0 at.% of Mn. The measurements were carried out at room temperature by exciting the films (deposited on crystalline quartz – which present a rather flat surface) with 632.8 nm photons. The features at ~475 and 525 cm^{-1} correspond to amorphous and crystalline Si, respectively. The signals at ~275, 300 and 320 cm^{-1} indicate the presence of the $MnSi_{1.7}$ silicide phase. The spectra have been normalized and vertically shifted for comparison.

the films. As a matter of fact, after crystallization, the ρ values are expected to change not only due to the Mn concentration, but also because of the relative amount of Si and $MnSi_{1.7}$ crystals.

The optical transmission spectra of some films considered in the present study are shown in Fig. 3. The spectra refer to films deposited on crystalline quartz substrates and without any treatment (as-deposited). The inset in Fig. 3 displays the average optical transmission of the films as a function of the Mn concentration: as-deposited and after thermal annealing at 750 and 900 °C. In this case, and for comparison reasons, the average optical transmission was considered at the arbitrarily chosen energy of 0.8 eV. The main experimental results in Fig. 3 can be summarized as: (1) except for very low Mn contents ([Mn] = 0.2 at.%), the insertion of manganese in the Si matrix decreases the optical transmission of the films, and (2) thermal annealing the films at 750 °C improves the optical transmission. These results are consistent with the electrical resistivity data in the sense that: the observed decrease in the optical transmission is associated with the presence of defects (more precisely, tail states), and thermal annealing of the films can promote some structural–electronic improvement (by reducing the density of defects) [8,20]. While the presence of crystallites (of Si or $MnSi_{1.7}$) affects the ρ values, the same is true for the optical properties of the SiMn films.

Related to the structural characteristics, Fig. 4 shows the Raman spectra of some of the studied SiMn films, deposited on *c*-quartz. According to Fig. 4, films as-deposited and thermally annealed up to 600 °C exhibit a broad and featureless scattering signal at ~475 cm^{-1}, characteristic of the amorphous silicon structure [22]. Thermal annealing at increasing temperatures (≥750 °C), in contrast, induces the crystallization of the films irrespective of the Mn content. In such a case, the spectra present a sharp and well-defined scattering signal at approx. 525 cm^{-1} because of the presence of Si crystallites [23]. At these annealing temperatures, the Mn-containing films also exhibit Raman features at ~275, 300 and 320 cm^{-1}, indicating the presence of the $MnSi_{1.7}$ silicide phase [24]. These contributions are evident in the films containing 4.2 at.% [Fig. 4(b)] and 20.0 at.% of Mn [Fig. 4(c)], after annealing at ≥750 °C and ≥600 °C, respectively. Another remarkable aspect in the spectra of Fig. 4(c) is the metallic behavior exhibited by the Si film containing 20.0 at.% of Mn, as-deposited [25]. Finally, it is important to mention that Raman measurements were also performed in the SiMn films deposited on *c*-Si substrates. While the observed trends are very much the same, the films deposited on *c*-Si tend to crystallize at slightly lower temperatures, reflecting the influence of the nature of the substrate on the crystallization process of *a*-Si films [26].

According to the literature [27], the $MnSi_{1.7}$ phase is representative of a group of several manganese Mn_xSi_y silicides, with y/x approximately equal to 1.7: Mn_4Si_7, $Mn_{15}Si_{26}$, $Mn_{27}Si_{47}$, etc. The crystallographic structure of these compounds is tetragonal, with about the same lattice parameter $a \sim 0.552$ nm, excepting the parameter c which is a function of x ($c = x\ c_0$, with $x \geq 4$ and $c_0 \sim 0.437$ nm) [28]. Related to their synthesis mechanism, Mn-silicides are known to develop from Mn layers deposited on *c*-Si in which case the growth of $MnSi_{1.7}$ is completed at about 600 °C [29] with a free energy of formation of ~6.7 kcal g^{-1} $atom^{-1}$ [30]. Considering the rich variety of Mn-silicides represented by $MnSi_{1.7}$, it is difficult to precisely identify the silicide phase only by Raman spectroscopy, and further structural investigation (by means of X-ray diffraction, for example) is needed. Therefore, the Mn-silicide of the present communication is generically identified by $MnSi_{1.7}$.

The analysis of the morphological results provided by SEM and AFM shows that the surface of all samples is rather flat and homogeneous, except for the films containing the highest amounts of Mn deposited on *c*-Si substrates. In these cases, the surfaces of the samples are covered by randomly distributed (sub-)micrometer structures which appearance is concurrent with the crystallization of the films. For practical reasons, and considering its magnetic activity [14,31], the morphological characteristics of only the SiMn film with [Mn] = 20.0 at.% (henceforth referred by $SiMn_{20\%}$) and annealed at temperatures ≥600 °C will be considered in detail.

Fig. 5 shows the SEM and AFM images of the $SiMn_{20\%}$ film after thermal annealing at 600, 750 and 900 °C. According to the micrographs the observed superficial structures present diameters in the ~750–1200 nm range and are ~300–400 nm high. Moreover, their distribution and typical dimensions are affected by the annealing temperature, as will be discussed in the following. The information provided by Raman spectroscopy and EDX measurements also

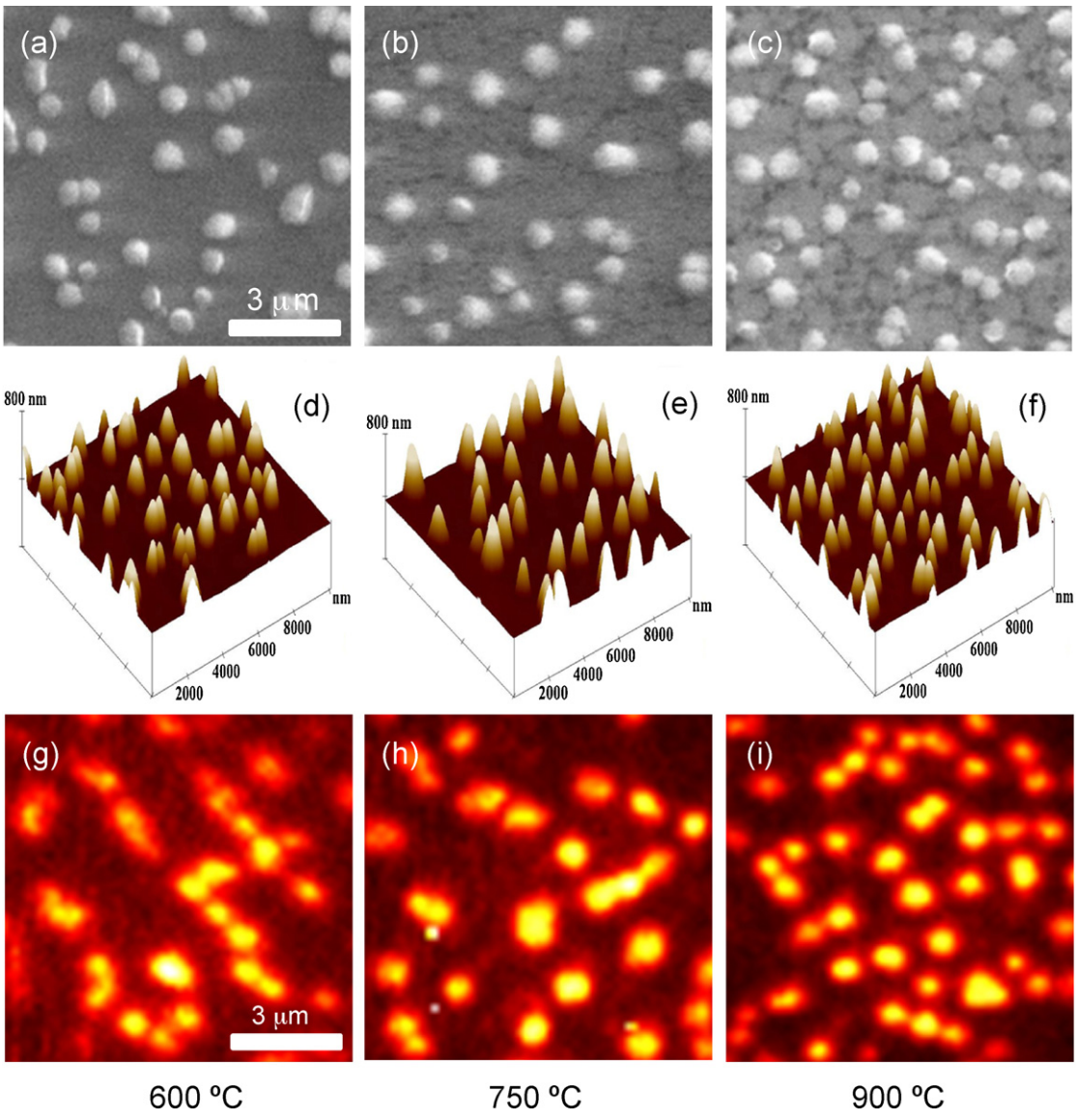

Fig. 5. SEM [(a)–(c)], AFM [(d)–(f)] and Raman images [(g)–(i)] of the $SiMn_{20\%}$ film thermally annealed at 600 [(a), (d), and (g)], 750 [(b), (e), and (h)] and 900 °C [(c), (f), and (i)], deposited on *c*-Si. At this specific Mn concentration, the crystallization of the sample coincides with the development of (sub-)micrometer structures randomly distributed on its surface, which density and typical dimension vary with the annealing temperature. All images correspond to regions of 10 μm × 10 μm.

indicates that the structures are essentially Mn-containing Si crystals (with a Mn concentration <17 at.%) surrounded by the $MnSi_{1.7}$ silicide phase [14].

Taking advantage of the high spatial localization and compositional characteristics of the observed superficial structures, they were further investigated by means of Raman imaging [32]. Towards this end, a sample surface area of ~15 μm in diameter was laser excited and the scattered light (after passing a bandpass filter tuned at $525 \pm 10\,cm^{-1}$, corresponding to crystalline Si) was directly imaged onto a charge-coupled device detector. The Raman images achieved from the $SiMn_{20\%}$ sample after thermal annealing at 600, 750 and 900 °C are shown in the lower part of Fig. 5. Despite the low spatial resolution provided by optical microscopy (~500 nm) [32], the Raman imaging results are consistent with those presented by SEM and AFM and indicate that the superficial structures correspond to Mn-containing Si crystals distributed all over the surface of the film. At this point, it is worth noting that crystalline Si can also exist outside of the observed superficial structures. In such a case, Si crystals present no special shape (at least within the spatial resolution provided by our microscopic resources) and their Raman intensity is very weak because of the presence of the $MnSi_{1.7}$ silicide phase and of a comparatively higher Mn content [14]. Finally, the Mn-free *a*-Si film also crystallizes after thermal annealing at ~750 °C [Fig. 4(a)], but no special features could be detected by SEM or AFM on its surface.

Concerning the development of the observed (sub-)micrometer structures on the surface of the $SiMn_{20\%}$ sample, a few comments are in order: (a) Mn species are faster diffusers in Si and, due to the very low energy of vacancy formation, the solid solubility of Mn in Si is extremely low (staying around 10^{-7}) [33], (b) the sequence of formation $MnSi \rightarrow MnSi_{1.7}$ starts at 400 °C and is almost completed at ~600 °C – the $MnSi_{1.7}$ phase being rather stable at increasing temperatures [29], (c) owing to a relatively small lattice mismatch (~1.8%) [34], the $MnSi_{1.7}$ silicide phase grows epitaxially on *c*-Si surfaces, and (d) Mn-silicide formation takes place mostly from the surface into the volume of the sample [35]. Combined with the current ensemble of experimental results, the previous information lead us to suggest the following mechanism for the development of the (sub-)micrometer structures on the surface of the present SiMn films: (1) as soon as the crystallization of *a*-Si begins (Fig. 4), it is

Table 1
Number (N) and mean individual area (area) of Mn-containing Si superficial structures as obtained from the SEM, AFM and Raman images shown in Fig. 5 (analyzed area of 10 μm × 10 μm). The data correspond to the structures present in a $SiMn_{20\%}$ film, deposited on *c*-Si, after thermal annealing at 600, 750 and 900 °C. The estimated error values take into account uncertainties of both the data analysis and experimental resolution of each technique.

Annealing temperature (°C)	SEM		AFM		Raman imaging	
	N	Area (μm^2)	N	Area (μm^2)	N	Area (μm^2)
600	37 ± 5	0.51 ± 0.03	37 ± 5	0.48 ± 0.01	30 ± 5	0.78 ± 0.05
750	30 ± 5	0.58 ± 0.03	32 ± 5	0.49 ± 0.01	26 ± 5	1.05 ± 0.05
900	54 ± 5	0.47 ± 0.03	58 ± 5	0.34 ± 0.01	46 ± 5	0.71 ± 0.05

accompanied by the diffusion of Mn and the formation of some Mn-silicide phase, (2) as the annealing temperature increases, there are Si crystallites dispersed along the film but, because of the higher diffusivity and lower solubility of Mn, most of the Si crystallites tend to accumulate on the surface of the sample, and (3) the whole process is made possible (or enhanced) by the interface with the *c*-Si substrate which takes into account the small lattice mismatch between Si and $MnSi_{1.7}$.

Whereas the previous reasoning partially explains the development of the (sub-)micrometer structures (Mn-containing Si crystals) on the surface of the SiMn films, their typical size and distribution vary with the annealing temperature (Fig. 5) and deserve further discussion.

The development of small crystalline structures instead of a continuous crystalline film – which is thermodynamically more stable – depends on experimental details such as: the deposition method and chemical aspects involved, the deposition rate and substrate temperature, and annealing conditions. Considering the adopted deposition method and conditions (conventional sputtering with the substrates at 150 °C), and taking into consideration our Raman data, an amorphous Si film containing Mn is the starting point of the samples under investigation. Hence, all structural–morphological changes verified in the present SiMn samples are exclusively due to the thermal annealing treatments. According to the classical theory of nucleation, the crystallization of an amorphous matrix relies on the presence of small crystalline units that are called nuclei or embryos [36]. When these crystalline units exceed a critical size, the free energy of the system is minimized, and crystallization takes place. In fact, this mechanism is believed to be at the origin of the crystallization process observed in systems involving the thermal annealing of either amorphous multilayers [37] or amorphous films doped with metallic species [26,38].

For the present samples, as the thermal annealing advances, crystalline Si and $MnSi_{1.7}$ phases are produced due to differences in the solubility and mobility of the foremost species. Owing to their different chemical–structural nature it is expected that the conditions leading to the effective formation of Si crystals and $MnSi_{1.7}$ are not the same. Indeed, the different energies required to form Si crystals or $MnSi_{1.7}$ (and their corresponding nuclei critical size) makes the former to adopt the shape of a (sub-)micrometer sized structure, whereas the latter is more like a continuous film – as experimentally observed (Fig. 5 and Ref. [14]). Depending on the annealing temperature, it is suggested that there is a competition between the growth of Si crystals and $MnSi_{1.7}$, which is also influenced by: sample thickness, the Mn concentration, the extent of the thermal treatment, the presence of defects such as microvoids or micro-imperfections, and film-substrate interfacial effects, for example [26,38]. These factors are also expected to determine the size, shape, and distribution of the Si crystals as well.

The typical size and distribution of the Mn-containing Si structures present in sample $SiMn_{20\%}$ after thermal annealing at 600, 750, and 900 °C are indicated in Table 1. The analysis took into account the data provided by the SEM, AFM and Raman imaging results of films deposited on *c*-Si substrates (Fig. 5) – all of them considering an analyzed area of 10 μm × 10 μm. Similar results (not shown) have been found in Si films with lower Mn concentrations in which the total number of Mn-containing Si crystals tends to be very reduced.

Considering the typical spatial resolution achieved with SEM, AFM, and Raman imaging the results shown in Table 1 are in good agreement. Moreover, the experimental data suggest that the number of superficial structures increases with the annealing temperature: from ~0.35 structures μm^{-2} at 600 °C, to ~0.55 structures μm^{-2} at 900 °C. Consistently, the average area (and, consequently, size) of the Mn-containing Si structures decreases with the temperature: from ~0.6 μm^2 at 600 °C to ~0.5 μm^2 at 900 °C. Such a behavior is consistent with the idea that increasing the annealing temperature induces the Mn diffusivity and, consequently, the probability to form the $MnSi_{1.7}$ phase in detriment of the Mn-containing Si structures. If that is correct, it is proposed that at even higher annealing temperatures (and/or longer annealing times) the sample will be transformed into a continuous film of $MnSi_{1.7}$ silicide covered with pure crystalline Si crystals on its surface.

4. Concluding remarks

In summary, this work contains a comprehensive study on sputter-deposited amorphous Si films with Mn in the ~0–20 at.% concentration range. After deposition, the samples were thermally annealed up to 900 °C and were examined by different techniques. The atomic composition of the samples was determined by EDX, RBS and XPS, and their structural–morphological characteristics were investigated in detail by Raman spectroscopy, SEM and AFM. Additional information was also achieved by optical transmission and electrical resistivity measurements. Based on the present experimental investigation it is possible to state that: (1) Mn species have been effective and controllably inserted into the amorphous Si matrix by the sputtering method which, allied to thermal annealing treatments, has proven to be a very convenient approach to produce the $MnSi_{1.7}$ phase; (2) both the Mn concentration and thermal treatment influence the properties of the studied SiMn films either inducing the development of crystalline structures or altering their optical–electronic characteristics; (3) although only the Si films with [Mn] = 0, 4.2, and 20.0 at.% have been discussed in detail (Fig. 4), after thermal annealing at ≥750 °C, all Mn-containing Si films exhibit the $MnSi_{1.7}$ silicide phase, which proportion scales with the [Mn]; (4) the crystallization of the films with the highest [Mn] is accompanied by the development of (sub-)micrometer structures randomly distributed on their surfaces; (5) these structures, essentially Mn-containing Si crystals, are believed to arise because of the low solubility and the fast diffusivity of Mn, and their main characteristics are credited to experimental factors such as annealing temperature, sample thickness, Mn concentration, annealing time, and film–substrate interfacial effects; (6) size distribution analysis suggest that, as the thermal annealing advances, the density of the Mn-containing Si structures increases while their average size shrinks; (7) in association with the magnetic activity exhibited by the $SiMn_{20\%}$ sample, we believe that the present set of experimental data adds relevant and useful

information towards the comprehension of Si-based magnetic materials.

Acknowledgements

The authors are indebted to Prof F.L. Freire Jr. (PUC – RJ) for the RBS analysis, and to Prof F. Alvarez and Dr J. Acuña (both at UNICAMP) for the XPS measurements. This work was financially supported by the Brazilian agencies FAPESP and CNPq.

Appendix A. Supplementary data

Supplementary data associated with this article can be found, in the online version, at doi:10.1016/j.matchemphys.2011.03.064.

References

[1] See, for example, I. Zutic, J. Fabian, S. das Sarma, Rev. Mod. Phys. 76 (2004) 323.
[2] T. Dietl, H. Ohno, Mater. Today 9 (2006) 18, and references therein.
[3] Y.D. Park, A.T. Hanbicki, S.C. Erwin, C.S. Hellberg, J.M. Sullivan, J.E. Mattson, T.F. Ambrose, A. Wilson, G. Spanos, B.T. Jonker, Science 295 (2002) 651.
[4] F.M. Zhang, X.C. Liu, J. Gao, X.S. Wu, Y.W. Du, H. Zhu, J.Q. Xiao, P. Chen, Appl. Phys. Lett. 85 (2004) 786.
[5] F. Bernardini, S. Picozzi, A. Continenza, Appl. Phys. Lett. 84 (2004) 2289.
[6] A.P. Li, C. Zeng, K. van Benthem, M.F. Chisholm, J. Shen, S.V.S.N. Rao, S.K. Dixit, L.C. Feldman, A.G. Petukhov, M. Foygel, H.H. Weitering, Phys. Rev. B 75 (2007) 201201.
[7] S. Zhou, K. Potzger, G. Zhang, A. Mucklich, F. Eichhorn, N. Schell, R. Grotzschel, B. Schmidt, W. Skorupa, M. Helm, J. Fassbender, Phys. Rev. B 75 (2007) 085203.
[8] See, for example, N.F. Mott, E.A. Davis, Electronic Processes in Non-Crystalline Materials, Clarendon Press, Oxford, 1979, p. 320.
[9] A. Lietoila, J.F. Gibbons, T.W. Sigmon, Appl. Phys. Lett. 36 (1980) 765.
[10] J.S. Williams, R.G. Elliman, Appl. Phys. Lett. 40 (1982) 266.
[11] S. Yada, S. Sugahara, M. Tanaka, Appl. Phys. Lett. 93 (2008) 193108.
[12] J. Deng, Y. Tian, S. Yan, Q. Cao, G. Liu, Y. Chen, L. Mei, G. Ji, Z. Zhang, J. Appl. Phys. 104 (2008) 013905.
[13] L. Zeng, A. Huegel, E. Helgren, F. Hellman, C. Piamonteze, E. Arenholz, Appl. Phys. Lett. 92 (2008) 142503.
[14] F.A. Ferri, M.A. Pereira-da-Silva, A.R. Zanatta, J. Phys. D: Appl. Phys. 42 (2009) 132002.
[15] G. Ottaviani, J. Vac. Sci. Technol. 16 (1979) 1112.
[16] H. Lange, Phys. Stat. Sol. B 201 (1997) 3.
[17] W.R. Runyan, T.J. Shaffner, Semiconductor Measurements and Instrumentation, McGraw-Hill, Quebecor/Fairfield, 1998, p. 111.
[18] S.M. Sze, Semiconductor Devices: Physics and Technology, John Wiley & Sons, Singapore, 1985, p. 1.
[19] D.R. Lide (Ed.), CRC Handbook of Chemistry and Physics, 84th ed., CRC Press, Boca Raton, Florida, 2003, Section 12.
[20] R.A. Street, Hydrogenated Amorphous Silicon, Cambridge University Press, Cambridge, 1991, p. 62.
[21] C. Krontiras, K. Pomoni, M. Roilos, J. Phys. D: Appl. Phys. 21 (1988) 509.
[22] J.E. Smith Jr., M.H. Brodsky, B.L. Crowder, M.I. Nathan, A. Pinczuk, Phys. Rev. Lett. 26 (1971) 642.
[23] P.A. Temple, C.E. Hathaway, Phys. Rev. B 7 (1973) 3685.
[24] J.L. Wang, W.F. Su, R. Xu, Y.L. Fan, Z.M. Jiang, J. Raman Spectrosc. 40 (2009) 335.
[25] L. Koudelka, N. Lusting, J.S. Lannin, Sol. Stat. Commun. 63 (1987) 163.
[26] See, for example, F.A. Ferri, A.R. Zanatta, I. Chambouleyron, J. Appl. Phys. 100 (2006) 094311.
[27] T.B. Massalski (Ed.), Binary Alloy Phase Diagrams, 2nd ed., ASM International, Materials Park, Ohio, 1990, p. 1.
[28] M. Tanaka, Q. Zhang, M. Taneguchi, K. Furuya, Surf. Sci. 532–535 (2003) 946.
[29] M. Eizenberg, K.N. Tu, J. Appl. Phys. 53 (1982) 6885.
[30] H. Tatsuoka, T. Koga, K. Matsuda, Y. Nose, Y. Souno, H. Kuwabara, P.D. Brown, C.J. Humphreys, Thin Solid Films 381 (2001) 231.
[31] The magnetic properties of the SiMn film ([Mn] = 20.0 at.%) was investigated by means of magnetic-force microscopy measurements carried out at room-temperature. Based on the experimental results, the magnetic activity is more intense near the Mn-containing Si structures and, because of the typical dimensions of the structures, occurs in the form of magnetic vortices. The observed magnetic activity was attributed to the formation of ferromagnetic Mn dimmers in combination with the presence of the $MnSi_{1.7}$ silicide phase. In such a case, the presence of $MnSi_{1.7}$ enhances the magnetization by mediating the exchange coupling between ferromagnetic Mn clusters.
[32] I.R. Lewis, in: H.G.M. Edwards (Ed.), Handbook of Raman Spectroscopy, Practical Spectroscopy Series, 28, CRC Press, New York, 2001, p. 191.
[33] E.R. Weber, Appl. Phys. A: Solids Surf. 30 (1983) 1.
[34] Y.C. Lian, L.J. Chen, Appl. Phys. Lett. 48 (1986) 359.
[35] T.S. Kamilov, D.K. Kabilov, I.S. Smiev, K.K. Khusnutdinova, R.A. Muminov, V.V. Klechkovskaya, Tech. Phys. 75 (2005) 140.
[36] W.A. Tiller, The Science of Crystallization – Microscopic Interfacial Phenomena, Cambridge University Press, Cambridge, 1991, p. 1.
[37] I. Honma, H. Komiyama, K. Tanaka, J. Appl. Phys. 66 (1989) 1170.
[38] F.A. Ferri, A.R. Zanatta, J. Appl. Phys. 104 (2008) 013534.